A DISTRIBUTED SHEAR AND FLEXURAL FLEXIBILITY MODEL WITH SHEAR-FLEXURE INTERACTION FOR R/C MEMBERS SUBJECTED TO SEISMIC LOADING

P.E. Mergos[1], A. J. Kappos[2]

[1] Graduate Student, Lab. of Concrete and Masonry Structures, Department of Civil Engineering, Aristotle University of Thessaloniki, Greece
[2] Professor, Lab. of Concrete and Masonry Structures, Department of Civil Engineering, Aristotle University of Thessaloniki, 54124 Greece
(tel: +30 2310 995743, e-mail: ajkap@civil.auth.gr)

SUMMARY

A beam-column type finite element for seismic assessment of R/C frame structures is presented. This finite element consists of two interacting, distributed flexibility sub-elements representing inelastic flexural and shear response. Following this formulation, the proposed model is able to capture spread of flexural yielding, as well as spread of shear cracking, in R/C members. The model accounts for shear strength degradation with inelastic curvature demand, as well as coupling between inelastic flexural and shear deformations after flexural yielding, observed in many experimental studies. An empirical relationship is proposed for evaluating average shear distortion of R/C columns at onset of stirrup yielding. The proposed numerical model is validated against experimental results involving R/C columns subjected to cyclic loading. It is shown that the model can predict well the hysteretic response of R/C columns with different failure modes, i.e. flexure-critical elements, elements failing in shear after flexural yielding, and shear-critical R/C members.

Keywords: finite element, distributed flexibility, shear-flexure interaction

INTRODUCTION

Most of the existing reinforced concrete (R/C) buildings have been designed prior to the introduction of modern seismic codes. Such buildings have nonconforming reinforcing details and often lack the strength and ductility to withstand major earthquakes. However, retrofitting of all these buildings is not feasible due to the very high costs involved. Therefore, refined assessment procedures are required to assess the performance and establish priorities for retrofit of existing buildings.

In recent years, nonlinear analysis procedures, although more complex and computationally demanding, have gained favor over the conventional linear elastic methods for the evaluation of existing structures. Nevertheless, the main focus of these procedures is on the flexural aspects of the response. Modeling of inelastic shear response and shear failure mechanisms, and particularly of their interaction with flexure, has been little explored, even more so in the case of members not satisfying the requirements of modern seismic codes.

Some researchers have attempted to explicitly include inelastic shear response in assessment of R/C structures [1-10]. The small number of such studies compared to those dealing with predominantly flexural response, should be attributed to the fact that determination of shear strength of R/C members, and especially of shear deformation characteristics, are still controversial issues. Advanced analytical procedures like the modified compression field theory (MCFT) [11] and the softened truss model [12] have been developed to predict shear force vs. shear deformation response. While these procedures are conceptually attractive, they have not yet been extended to cope successfully with degradation of shear strength in plastic hinge regions [13]. Moreover, the computational effort involved may limit their application, especially for response history analyses of complete multi-storey structures.

Ricles et al. [5] and Cosenza et al. [10] used the shear strength model by Priestley et al. [14] to describe shear strength degradation with increasing flexural ductility demand of a macro-element column model. While these models predict shear failure with reasonable accuracy and computational efficiency, they are not capable of modeling coupling of inelastic flexural and shear deformations observed in several experimental studies [15, 16]. Moreover, the vast majority of finite element models developed so far for inelastic shear response analysis of R/C structures, have adopted the single shear spring approach [1], which is equivalent to assuming a constant value of shear stiffness along the entire member.

In the light of the above, a new finite element for R/C beam-column members is proposed in this paper. This finite element belongs to the class of phenomenological, 'member type', models. It consists of two sub-elements with distributed flexibility, representing inelastic flexural and shear response. The two sub-elements are connected by equilibrium and interact throughout the analysis to capture the shear-flexure interaction effect. The total flexibility of the finite element is calculated as the sum of the flexibilities of its sub-elements, and can be inverted to produce the element

stiffness matrix. The components of the aforementioned finite element, as well as their interaction, are described in the following sections. The proposed element is then used to predict the hysteretic response of R/C column specimens with different failure modes (flexure-critical, failing in shear after flexural yielding, and shear-critical).

FLEXURAL SUB-ELEMENT

This sub-element is used for modeling the flexural behavior of an R/C member subjected to cyclic loading before, as well as after, yielding of the reinforcement. It consists of a set of rules governing the hysteretic moment-curvature (M-φ) behavior of the member end sections, and a spread plasticity model describing flexural stiffness distribution along the entire member.

M-φ relationship for member end sections

The M-φ relationship at each end section of the member is described by the primary curve and the rules determining its hysteretic behavior. The primary M-φ relationship is derived using standard flexural analysis of the critical cross section, with appropriate constitutive laws for concrete and steel. The relationship is then approximated by a bilinear (elastoplastic with strain hardening) curve. It is believed that a bilinear curve better represents the behavior of existing R/C members, especially old ones, which are very likely to be already cracked due to gravity and/or environmental loading, as well as previous earthquakes.

The multi-linear, 'yield-oriented' with slip, hysteretic model of Sivaselvan and Reinhorn [17] was adopted herein for describing M-φ behavior. This model is an extension of the Park et al. [18] model; it accounts for stiffness degradation, strength deterioration, pinching effect, and non-symmetric response. However, the aforementioned model is based on a trilinear envelope curve. Hence, its hysteretic rules were appropriately modified by the writers to be compatible with a bilinear sceleton curve. The latest was achieved by matching the ends of the elastic branch with the positive and negative yielding point of the hysteretic model and not the respective cracking points, as is the case in the original model.

Flexural spread plasticity model

It is known that under seismic loading inducing inelastic behavior, sections along the element will exhibit different stiffness characteristics depending on the degree of inelasticity. To capture the variation of the section flexibility along the R/C member, a spread plasticity formulation has to be developed. A number of researchers have developed flexural, spread plasticity, elements [3, 18, 19, 20, 21]. The flexural sub-element presented herein is based primarily on the model by Valles et al. [21].

The stiffness distribution along the member is assumed to have the shape of Fig. 1, where: L is the length of the member; EI_A and EI_B are the current flexural rigidities of the sections at the ends A and B, respectively; EI_o is the stiffness at the intermediate part of the element; α_A and α_B are the 'yield penetration' coefficients. The flexural rigidities EI_A and EI_B are determined from the M-φ hysteretic relationship of the corresponding end sections. In this study, it is assumed that the state (loading, unloading, reloading) and the stiffness of the spread plastic zone is controlled by the state and the stiffness of the section at the end of the member. The yield penetration coefficients specify the proportion of the element where the acting moment is greater than the end section yield moment. These coefficients are first calculated for the current moment distribution and then compared with the previous maximum penetration lengths; the yield penetration lengths cannot be smaller than their previous maximum values ('model with memory') [21].

The flexural spread plasticity model presented in this work differs from the model of Valles et al. [21] in that constant rigidity is assumed along the yield penetration lengths, and nonlinear moment distribution due to possible gravity load effects is taken into account in calculating the yield penetration coefficients (Fig. 1); the latter feature is particularly important in the case of beams.

Having established the stiffness distribution along the R/C member at each step of the analysis, the coefficients of the flexibility matrix of the flexural subelement can be derived from the following expressions (derived by applying the principle of virtual work to the variable cross-section element of Fig. 1).

$$f_{11}^{flex} = \frac{\left(4EI_AEI_B + 4\cdot\left(EI_o\cdot EI_B - EI_A\cdot EI_B\right)\cdot\left(3a_A - 3a_A^{\,2} + a_A^3\right) + 4\cdot(EI_o\cdot EI_A - EI_A\cdot EI_B)\cdot a_B^3\right)\cdot L}{12\cdot EI_A\cdot EI_B\cdot EI_o} \quad (1)$$

$$f_{12}^{flex} = \frac{\left(-2EI_AEI_B - 2\cdot\left(EI_o\cdot EI_B - EI_A\cdot EI_B\right)\cdot\left(3a_A^{\,2} - 2a_A^3\right) - 2\cdot\left(EI_o\cdot EI_A - EI_A\cdot EI_B\right)\cdot\left(3a_B^{\,2} - 2a_B^3\right)\right)\cdot L}{12\cdot EI_A\cdot EI_B\cdot EI_o} \quad (2)$$

$$f_{22}^{flex} = \frac{\left(4EI_AEI_B + 4\cdot\left(EI_o\cdot EI_A - EI_A\cdot EI_B\right)\cdot\left(3a_B - 3a_B^{\,2} + a_B^3\right) + 4\cdot(EI_o\cdot EI_B - EI_A\cdot EI_B)\cdot a_A^3\right)\cdot L}{12\cdot EI_A\cdot EI_B\cdot EI_o} \quad (3)$$

SHEAR SUB-ELEMENT

The shear sub-element represents the hysteretic shear behavior of the R/C member prior and subsequent to shear cracking. The shear sub-element has been designed in a similar way to the flexural element described above. It consists of a set of rules determining V-γ (shear force vs. shear distortion) hysteretic behavior of the member end regions, and a shear spread plasticity model defining shear stiffness distribution along the entire member. In this study, shear distortion, γ, is defined as the average shear deformation along the discrete regions (cracked or uncracked) of the shear sub-element. The V-γ relationship of each member end region is determined by the primary curve and the rules governing its hysteretic behavior. Initially, the backbone curve is calculated without including shear-flexure interaction effects (initial backbone). Then, shear flexure interaction effects are modeled by assigning an appropriate analytical procedure. The individual components of the shear sub-element are described in more detail in the following.

End region V-γ envelope curve without shear flexure interaction effect

The V-γ primary curve consists of three branches (Fig. 2), but only two different slopes, as explained later on. The first branch connects the origin and the shear cracking point, which is defined as the point where the nominal principal tensile stress exceeds the mean tensile strength of concrete. Adopting the procedure suggested by Sezen and Moehle [22], the shear force at cracking is calculated as

$$V_c = \frac{f_{ctm}}{L_s / h}\sqrt{1+\frac{N}{f_{ctm}\cdot A_g}}\cdot 0.80 A_g \qquad (4)$$

wherein f_{ctm} is the mean concrete tensile strength, N is the compressive axial load, L_s/h is the shear span ratio and A_g is the gross area of the concrete section. To take into account a parabolic shear stress distribution along the depth of the cross section, the initial shear stiffness GA_{eff} is calculated by Eq. (5) where G is the (elastic) shear modulus.

$$GA_{eff} = G\cdot\left(0.80 A_g\right) \qquad (5)$$

The second and third branches of the initial primary curve have the same slope and connect the shear cracking point to the point corresponding to the onset of yielding of

transverse reinforcement (V_{uo}, γ_u). The latter is taken as the 'failure' point in this approach that does not include the post-failure range of response. The rationale behind ignoring this range is that poorly detailed R/C columns will lose shear capacity rapidly after reaching this point (e.g. see Pincheira et al. [7]), while properly detailed R/C members are very unlikely to exceed this point. The second and third branches are separated at the point corresponding to flexural yielding (V_y, γ_y). This approach was adopted in order to distinguish hysteretic shear behavior before and after flexural yielding [23].

The mean shear distortion at the onset of transverse reinforcement yielding, γ_u, is estimated using the truss analogy approach proposed by Park and Paulay [24] and Kowalsky and Priestley [25]. According to this approach, in a cracked member the shear deformation will arise from the extension of transverse reinforcement and the compression of the diagonal compression struts; the resulting shear distortion, γ_s, after shear cracking is

$$\gamma_s = \frac{V_{cr}}{GA_{eff}} + \frac{V_s}{(d-d')} \cdot \left(\frac{s}{E_s \cdot A_w \cdot \cot\theta^2} + \frac{1}{E_c \cdot b \cdot \sin\theta^3 \cdot \cos\theta \cdot \cot\theta} \right) \quad (6)$$

where: A_w is the area of transverse reinforcement oriented parallel to the shear force; d-d' is the distance measured parallel to the applied shear between centers of transverse reinforcement; s is the spacing of transverse reinforcement; b is the width of the cross section; E_c is the elastic modulus of concrete and E_s the elastic modulus of steel; V_s is the shear force resisted by the transverse reinforcement, and θ the angle defined by the column axis and the direction of the diagonal compression struts. Then, γ_u, is calculated by Eq. (6) by setting V_s equal to the shear strength contributed by the transverse reinforcement, V_w, given by

$$V_w = \frac{A_w \cdot f_{yw} \cdot (d-d') \cdot \cot\theta}{s} \quad (7)$$

where f_{yw} is the yield stress of transverse reinforcement

Although the aforementioned procedure is based on a rational approach, calibration studies by the writers showed that it does not account accurately enough for the influence of the axial load and member aspect ratio on γ_u. Available experimental data regarding average shear distortion at the onset of stirrup yielding are very limited. Even when shear displacements at the tip of a shear critical member (Δ_{shear}) are

recorded, determination of γ_u is not a straightforward procedure. In R/C members where flexural yielding has occurred prior to stirrup yielding, shear displacements continue to increase after flexural yielding, while shear force remains almost constant [16]. Similarly, in well detailed R/C members, shear displacements may increase substantially after yielding of the transverse reinforcement without significant drop in shear strength. Hence, determination of γ_u can be achieved only if there is a clear peak on the V-Δ_{shear} envelope curve (i.e. if rapid shear strength degradation occurs immediately after flexural yielding in shear-flexure critical R/C members, or shear strength degradation occurs shortly after attainment of maximum shear strength in shear critical R/C members).

Five R/C column tests were found in the literature, for which γ_u could be determined by the V-Δ_{shear} relationship. Table 1 summarizes the estimated values of γ_u as well as the aspect ratios and normalized axial loads, $\nu=N/(f_c \cdot A_g)$, on the members.

To complement the aforementioned experimental data, a simple procedure is proposed herein, whereby γ_u can be defined without knowing the V-Δ_{shear} envelope curve. The proposed methodology can be applied only to R/C members failing in shear without yielding of the longitudinal reinforcement and only when rapid shear strength degradation occurs shortly after reaching maximum shear strength. At maximum shear strength, V_u^o, the total displacement Δ_{max}^{tot} can be considered as the sum of three deformation components [28]; the flexural component, Δ_{max}^{fl}, shear component, Δ_{max}^{sh}, and anchorage slip component, Δ_{max}^{sl}. Hence

$$\gamma_u = \frac{\Delta_{\max}^{sh}}{L_s} = \frac{\left(\Delta_{\max}^{tot} - \Delta_{\max}^{fl} - \Delta_{\max}^{sl}\right)}{L_s} \tag{8}$$

Δ_{max}^{tot} can be determined from the experimental shear force vs. total displacement envelope curve. Furthermore, since the element has not yielded in flexure, Δ_{max}^{fl} and Δ_{max}^{sl} can be calculated, with adequate accuracy, by linear interpolation between zero displacement and the respective displacement corresponding to first yielding of longitudinal reinforcement.

$$\Delta_{\max}^{fl} = \frac{V_{uo}}{V_y} \cdot \Delta_y^{fl} \tag{9}$$

$$\Delta_{\max}^{sl} = \frac{V_{uo}}{V_y} \cdot \Delta_y^{sl} \tag{10}$$

where Δ_y^{fl} and Δ_y^{sl} are the flexural and anchorage slip displacements of the R/C member at first yielding of longitudinal reinforcement. Δ_y^{fl} can be determined by a M-φ analysis of the critical section of the member, and Δ_y^{sl} by an empirical formula based on test results [29]

$$\Delta_y^{fl} = \varphi_y \cdot \frac{L^2}{3} \tag{11}$$

$$\Delta_y^{sl} = \frac{0.13 \cdot \varphi_y \cdot d_b \cdot f_y \cdot L}{\sqrt{f_c}} \tag{12}$$

where: φ_y is the curvature of the critical cross section at first yielding of longitudinal reinforcement; d_{bl} is the diameter of a single longitudinal reinforcement bar; f_{yl} is the yield stress of longitudinal reinforcement, and f_c the compression strength of concrete. By combining Eqs (8) to (12), determination of γ_u is feasible. In all cases, it should be checked that the contributions of Δ_{max}^{fl} and Δ_{max}^{sl} to Δ_{max}^{tot} remain small, to avoid additional errors caused by the estimation of these components.

The methodology described above was applied to five (additional) R/C members. Table 2 summarizes the estimated values of γ_u, as well as the members aspect ratios and normalized axial loads. All ten specimens of Tables 1 and 2 can be considered as R/C columns (symmetrically reinforced), tested with or without axial load under uniaxial loading. All columns had rectangular cross section apart from test specimen C5A which had a circular cross section. Nine out of ten specimens were subjected to cyclic loading, while column 2CLD12M was subjected to monotonic loading during the last stage of the experiment. Normalized axial loads ranged from 0 to 0.60, while shear span ratios varied from 1.1 to 3.2.

Regression analyses showed that best correlation with experimental results was achieved when in calculating γ_u from Eqs. (6) and (7), the angle θ was taken equal to 35^o (unless limited to larger angles by the potential corner-to-corner crack) and the derived value was then multiplied by two modification factors. The first modification factor, κ, takes into account the influence of the axial load and is given by

$$\kappa = 1 - 1.03 \cdot \nu \tag{13}$$

The second modification factor, λ, represents the influence of the column aspect ratio and is given by the following expression

$$\lambda = 5.41 - 1.13 \cdot \left(\frac{L_s}{h} \right) \geq 1 \qquad (14)$$

Fig. (3) shows the comparison between analytical predictions by using Eqs. (6) and (7) with the modification factors κ and λ and the experimental values of γ_u. The median of the ratio of experimental to calculated values is 0.99 and the coefficient of variation 16.9%. In general, it can be said that the proposed formula correlates well with experimental results. However, it should be recalled that this formula is based on a very limited set of data.

Regarding shear strength, V_u, the approach proposed by Priestley et al. [14] is invoked, which has been developed for both circular and rectangular columns. According to this approach, V_u is given by

$$V_u = k \cdot \sqrt{f_c} \cdot \left(0.80 A_g\right) + N \cdot \tan a + \frac{A_w \cdot f_{yw} \left(d - d'\right) \cdot \cot \theta}{s} \qquad (15)$$

wherein k is a parameter depending on the curvature ductility demand as shown in Fig. (4), and α is the angle between the column axis and the line joining the centers of the flexural compression zones at the top and bottom of the column. For the initial shear primary curve, V_{uo} is derived by setting in Eq. (15) the value of k corresponding to curvature ductility demand $\mu_\varphi \leq 3$ (i.e. no strength degradation).

It is worth noting at this point that alternative procedures for deriving the V- γ backbone curve from refined analysis, for instance using the MCFT, were found to fail to capture shear strength degradation effects during cyclic loading [7].

Shear-flexure interaction

As implied by Eq. (15), shear strength decreases as curvature ductility demand increases. So far, in the vast majority of nonlinear analyses of R/C structures, this effect was taken into account by using, conservatively, the lower bound of shear strength. However, this approach has proven to be in many cases excessively conservative [13]. In the present study, shear strength degrades according to the current maximum curvature ductility demand. This is achieved using the following procedure.

First, at each time step i of the analysis, maximum curvature ductility demand of the critical cross section j (j=A,B), $\mu^i_{\varphi j,max}$, of the critical cross section of the flexural sub-element is defined. Then, the corresponding k^i_j factor is determined from

Fig. (4) and this factor is introduced into Eq. (15) to calculate current shear strength, $V_{u,j}^{i}$; hence the shear strength degradation is

$$DV_{u,j}^{i} = V_{uo,j} - V_{u,j}^{i} \tag{16}$$

This shear strength degradation is then modeled by reducing the ordinate of the backbone curve of the respective end section of the shear sub-element, as shown schematically in Fig. 5.

In order to reset equilibrium, the shear force increment at the time next step i+1, ΔV_j^{i+1}, is calculated by the total moment distribution at this time step minus the respective shear force of the previous time step, V_j^i. Assuming uniform gravity load distribution, we obtain

$$\Delta V_A^{i+1} = -\frac{q \cdot L}{2} + \frac{\left(M_A^{i+1} - M_B^{i+1}\right)}{L} - V_A^i \tag{17}$$

$$\Delta V_B^{i+1} = \frac{q \cdot L}{2} + \frac{\left(M_A^{i+1} - M_B^{i+1}\right)}{L} - V_B^i \tag{18}$$

Assuming that the end section of the shear sub-element still remains in the loading phase, the shear force increments calculated by Eqs (17)-(18) give rise to the respective shear strain increments, $\Delta\gamma_j^{i+1}$, defined by Eq. (19) and shown schematically in Fig. 5.

$$\Delta\gamma_j^{i+1} = \frac{\Delta V_j^{i+1}}{GA_1} \tag{19}$$

Combining the analytical procedure shown in Fig. (5) and the relationship between curvature ductility demand and strength of concrete shear resisting mechanisms presented in Fig. (4), yields the modified shear primary curve shown in Fig. 6; in this figure hardening of the flexural primary curve has been exaggerated for illustration purposes. Furthermore, it is assumed that curvature ductility capacity of the critical cross section exceeds the value of 15 (which is often not the case in old-type members) and that the element fails in shear *after* yielding in flexure.

As can be seen in Fig. 6, by adopting the analytical procedure described above, coupling between inelastic flexural and shear displacements is achieved. More particularly, it is observed that shear displacements increase more rapidly when curvature ductility demand exceeds the value of 3. This increase is sharper for $3<\mu_\varphi\leq 7$ and becomes smoother for $7<\mu_\varphi\leq 15$ (cf. Fig. 4). Finally, for $\mu_\varphi>15$, shear

displacements tend to increase at the same rate as they do for $\mu_\varphi \leq 3$. In all cases, by using this analytical procedure, shear deformation at shear failure will be equal to γ_u.

The shape of the modified shear primary curve is in accordance with the truss analogy approach [24, 25]. Based on this approach, shear distortion in a cracked member is analogous to the shear force resisted by the stirrups, V_s. According to Priestley et al. [14], after flexural yielding, shear force resisted by the concrete mechanisms, V_c, reduces and shear force resisted by the stirrups, V_s, increases in order to maintain equilibrium. By increasing V_s, shear distortions of the R/C member, γ_s, also increase, as it is clear from Eq. (6), while shear demand remains almost constant since it is controlled by flexural yielding. The rate of increase of V_s is higher when $3<\mu_\varphi \leq 7$ than when $7<\mu_\varphi \leq 15$ since the reduction of V_c is sharper in the former case, as can be seen in Fig. 4. This explains why it is $GA_2 \leq GA_3$ in the modified shear primary curve illustrated in Fig. 6. When μ_φ becomes higher than 15, V_c no longer degrades. Consequently, V_s increases only due to the respective increase in shear demand. This is the reason why after $\mu_\varphi > 15$ the slope of the modified shear primary curve becomes again equal to GA_1.

Hysteretic shear behavior

Hysteretic shear behavior was modeled using the proposals by Ozcebe and Saatcioglu [23] as a basis, with several modifications and improvements. Although this hysteretic model has been calibrated against experimental results and was found to yield a reasonable match, it has not been designed with a view to being incorporated in a dynamic nonlinear analysis framework. Therefore, extension and refinements were necessary, as discussed in the following.

The first modification is a simplification regarding the slope of unloading branches. According to Ozcebe and Saatcioglu [23], if V_y has been exceeded at least once, unloading stiffness is different above and below the cracking load (Fig 7a). This increases significantly the complexity of the model without a commensurate enhancement in the quality of the results. Hence, it is suggested by the writers that an average value for the unloading stiffness be used, as shown in Fig. 7(a). Furthermore, the equation giving the unloading stiffness in that hysteretic model may in some cases yield numerical instability problems like the one depicted in Fig. 7(b). In this case, it is suggested that the minimum unloading stiffness be defined by the vertex point

(onset of unloading branch) in the quadrant where unloading is taking place and the cracking point in the opposite quadrant (Fig. 7b).

The second development is a modification regarding the reloading branches. According to Ozcebe and Saatcioglu [23], if V_{cr} has been exceeded in the direction of loading, reloading up to V_{cr} will follow a straight line passing through a reference point (**P)** shown in Fig. 8(a). However, the equation defining the ordinate of this point may sometimes yield values lower or slightly greater than the cracking load. This may cause the numerical instability problems shown in Figures 8(a) and 8(b). To avoid these numerical problems, it is suggested that in the aforementioned cases the reference point **(P)** will be a point on the unloading branch in the direction of loading, which initiates at the load reversal point with the largest previous shear deformation, having as ordinate the shear force corresponding to the cracking load in the direction of loading.

Shear spread plasticity model

In the majority of nonlinear dynamic analyses of R/C structures, the single shear spring approach has been adopted to take into account inelastic shear behavior of R/C members. This is equivalent to assuming constant shear stiffness along the entire member. However, this may not be the case for various reasons, some of them being:

- In beam elements, shear force varies along the length of the member due to gravity loading.
- The two ends of the member may not have the same shear reinforcement or section dimensions.
- Shear-flexure interaction effect may be different at the two ends of the member.

Hence, a shear spread plasticity model would be attractive in all these cases. The first spread plasticity model for shear was proposed by the second writer and his associates [34]. In the shear sub-element proposed herein, the aforementioned model has been improved in several respects.

The shear rigidity distribution along the member is assumed to have the form shown in Fig. 9, where GA_A and GA_B are the current shear rigidities of the regions at the ends A and B, respectively; GA_o is the shear stiffness at the intermediate part of the element; α_{As} and α_{Bs} are the shear cracking penetration coefficients, which specify

the proportion of the element where the acting shear is greater than the shear cracking force of the end section. These coefficients are calculated as follows:

When acting shear force at end A is greater than cracking shear ($|V_A| \geq |V_{A,cr}|$), α_{As} is given by Eq. (20). Similarly, when $|V_B| \geq |V_{B,cr}|$, α_{Bs} is given by Eq. (21). Otherwise, these coefficients are taken equal to zero. When shear forces at both ends are of the same sign ($V_A \cdot V_B \geq 0$) and they are greater than the respective cracking shears (this is the typical case for column elements after shear cracking), it is assumed in this study that $\alpha_{As}=\alpha_{Bs}=0.5$.

$$\alpha_{As} = \frac{V_A - V_{A,cr}}{V_A - V_B} \leq 1 \tag{20}$$

$$\alpha_{Bs} = \frac{V_B - V_{B,cr}}{V_B - V_A} \leq 1 \tag{21}$$

The shear cracking penetration lengths are first calculated for the current shear distribution, then compared with the previous maximum penetration lengths, and cannot be smaller than the latter ('model with memory'). After determining the distribution of GA along the R/C member at each step of the analysis, the coefficients of the flexibility matrix of the shear sub-element are given by

$$f_{ij}^{shear} = \frac{a_{As}}{GA_A \cdot L} + \frac{1 - a_{As} - a_{Bs}}{GA_o \cdot L} + \frac{a_{Bs}}{GA_B \cdot L} \quad \text{where i,j=1,2} \tag{19}$$

CORRELATION WITH EXPERIMENTAL RESULTS

The proposed member-type model was implemented in a computer program (IDARC2D) for the nonlinear dynamic analysis of 2D R/C structures [21]. To validate the model, the program was used to simulate the hysteretic response of several R/C members tested under cyclic loading; results for a flexure-critical element, an element failed in shear after flexural yielding, and a shear-critical element are presented herein. It must be noted that at this stage of development, bond slip effects are not modeled directly, but rather slip is taken into account indirectly, first by adding the empirical yield penetration length $0.24 f_{yl} \cdot d_{bl} / \sqrt{f_c}$ [33], and second by using parameters corresponding to moderate degradation in the flexural hysteretic rules.

Flexure-critical R/C member

Lehman and Moehle [35] tested five circular R/C bridge columns, typical of modern construction, under uniaxial displacement-controlled lateral load reversals. The principal variables of the testing program were shear span ratio and longitudinal reinforcement ratio. Herein, the specimen designated as 415 is examined. This specimen had a shear span ratio of 4 and longitudinal reinforcement ratio 1.5%. The applied axial load was 654kN (ν=0.07). The volumetric ratio of shear reinforcement was 0.7% with configuration as shown in Fig. 10(a). Concrete strength was 31MPa and yield strengths of longitudinal and transverse reinforcement were 462 and 607 MPa, respectively.

This specimen was dominated by flexure, exhibiting stable hysteretic behavior until failure. Fig. 10(a) shows the experimental and analytical lateral load vs. total displacement relationship of the specimen. It is seen that the proposed analytical model predicts well the experimental behavior up to maximum response. In Fig. 10(b), shear demand and capacity are illustrated as a function of the curvature demand at the end section of the member. Although shear capacity drops significantly due to inelastic flexural demand, it remains constantly above the shear demand; hence, consistently with the test results, no shear failure was predicted.

Fig. 10(c) presents the shear force vs. shear strain relationship predicted by the analytical model. It is clear that this behavior is characterized by pinching. On the same figure, the initial backbone curve of this relationship is illustrated. It can be seen that after flexural yielding, hysteretic shear response deviates from the initial envelope. Shear displacements increase significantly, while shear demand remains almost constant. Nevertheless, shear strain remains always smaller than γ_u since no shear failure has taken place. This coupling between inelastic flexural and shear displacements was achieved by the shear-flexure interaction procedure described in the previous section.

Finally, Fig. 10(d) shows the 'time-history' of the displacement components. It is clear that for the R/C member under consideration, flexure and bond-slip govern the response. It is pointed out that at maximum displacement demand, shear displacement represents only 3% of the total displacement. This agrees well with the experimental observations [35].

Flexure-shear critical R/C member

Lynn et al. [36] tested 8 full scale columns, representative of old type construction, having widely-spaced perimeter hoops with 90 degree bends, with or without intermediate hoops and longitudinal reinforcement with or without lap splices. Herein, the specimen designated as 2CLH18 is examined. The clear height of the specimen was 2946mm and it was subjected to lateral load deformation cycles in double bending under a constant axial load of 503kN (ν=0.07). Transverse reinforcement was placed at a spacing of 457mm with the configuration shown in Fig. 11(a). Concrete strength was 33.1MPa and yield strengths of longitudinal and transverse reinforcement were 331MPa and 400MPa, respectively. In the following, shear strength V_u was calculated by Eq. (15), where the contribution of stirrups was reduced by half due to the absence of the 135^o hook [37].

Fig. 11(a) shows the experimental and analytical lateral load vs. total displacement relationship for the aforementioned specimen. It can be seen that the analytical model is able to represent very well the experimental results. The specific R/C member exhibited a rather complex behavior, yielding in flexure and then failing in shear due to drop of its shear capacity caused by shear-flexure interaction. It is important to note that the analytical model was able to capture this response and predict the shear failure of the member at a displacement of 38mm. This is clear also from Fig. 11(b) which presents the shear demand and capacity variation with the curvature demand at the critical cross-section of the member. It can be seen that prior to flexural yielding, shear capacity is significantly higher than the corresponding demand. However, when curvature ductility demand exceeds the value of 3, shear capacity degrades significantly and eventually reaches shear demand at the displacement of 38mm, at which stage shear failure occurs.

Fig. 11(c) illustrates the shear force vs. shear strain hysteretic relationship. It can be seen that, when curvature ductility demand exceeds the value of 3, shear distortions increase significantly, while shear demand remains almost constant since it is controlled by flexural yielding. Eventually, shear failure occurs when the shear strain reaches γ_u, which was found to be 0.24%.

Finally, Fig. 11(d) shows the time-history of the displacement components. Again, it is clear that flexure and slip govern the response. At maximum displacement demand, shear displacement represents only 9% of the total displacement; this may be

attributed to the relatively high shear span ratio (3.2) of the column.

Shear-critical R/C member

A shear critical R/C element fails in shear before yielding in flexure. This represents a special case that lies beyond the scope of the proposed rules for determining the backbone curve for inelastic shear. Furthermore, the hysteretic model adopted as a basis for shear [23] has not been designed for shear critical R/C elements. It is proposed by the writers that in these cases the second branch of the backbone curve be 'removed' by setting the end of this branch slightly greater than the cracking load. In this way, maximum pinching and stiffness degradation caused by inelastic shear displacements are assured.

Aboutaha et al. [33] tested eleven large-scale columns to examine the effectiveness of various types of steel jackets for improving the strength and ductility of columns with inadequate shear resistance. The shear span ratio of the columns was equal to 1.33. All columns were tested without axial load. Three columns were tested as basic unretrofitted specimens. Herein, the unretrofitted specimen designated as SC9 is examined. This specimen was subjected to uniaxial excitation in its strong direction. Transverse reinforcement was placed at a spacing of 406mm with the configuration shown in Fig. 12(a). Concrete strength was 16MPa; yield strengths of longitudinal and transverse reinforcement were 434MPa and 400MPa, respectively.

Fig. 12(a) shows the experimental and analytical lateral load vs. total displacement relationship of the aforementioned specimen. It can be seen that the analytical model is able to capture adequately the pre-peak experimental response. The small underestimation of shear strength is justified given the great number of uncertainties involved in calculating shear strength of squat R/C elements. It is very encouraging that the analytical model was able to predict accurately the displacement at which shear strength starts to degrade rapidly. This was achieved by the correct prediction of γ_u using Eqs. (6) and (7) with the modification factors of Eqs. (13) and (14).

Fig. 12(b) presents the shear force vs. shear strain relationship predicted by the analytical model. It is clear that this relationship is characterized by significant pinching and poor energy dissipation. The analytical model was able to predict that no flexural yielding developed during the experiment. Hence, shear hysteresis follows the initial backbone curve over the whole range of the response. Fig. 12(c) shows a comparison of the analytical prediction and the experimental behavior when shear is

not modeled explicitly. It is clear from this figure that ignoring inelastic shear behavior may lead to totally erroneous results regarding both strength and deformation.

Finally, Fig. 12(d) presents the time-history of displacement components. As expected, shear displacements govern the response of this R/C member. At maximum displacement demand, shear displacement represents about 75% of the total displacement, emphasizing again the need for accurate modeling of these displacements in squat R/C elements.

CONCLUSIONS

A distributed shear and flexural flexibility model with shear-flexure interaction for seismic assessment of R/C structures has been developed. The model is based on simple analytical procedures, which ensure reasonable accuracy and computational efficiency. The proposed model was implemented into the nonlinear static and dynamic analysis program IDARC2D. It was then used to simulate the nonlinear response of flexure-critical, flexure-shear critical, and shear-critical R/C columns subjected to cyclic lateral loads.

Good agreement between analytical and experimental results was generally observed. However, further refinement of the model is clearly possible. This can be achieved by the direct inclusion of bond-slip effects as an independent component of the model. Even at this stage of development, the simplicity and computational efficiency of the proposed model and its ability to reasonably capture the behavior of actual R/C members with different failure modes, make it a valuable tool for the assessment of the seismic behavior of R/C structures, especially those with non-conforming detailing.

Notation

The following symbols are used in this paper

A_g	=	gross area of the concrete section
A_w	=	area of transverse reinforcement
b	=	width of the cross section
d-d’	=	distance measured parallel to the applied shear between centers of transverse reinforcement
d_{bl}	=	diameter of a single longitudinal reinforcement bar
DV_u	=	current total shear strength degradation
E_c	=	elastic modulus of concrete
E_s	=	elastic modulus of steel
EI_A	=	current flexural rigidity of the section at end A
EI_B	=	current flexural rigidity of the section at end B
EI_o	=	flexural rigidity at the intermediate part of the element
f_c	=	concrete strength
f_{ctm}	=	mean concrete tensile strength
f_{ij}^{flex}	=	flexibility coefficients of the flexural sub-element
f_{ij}^{shear}	=	flexibility coefficients of the shear sub-element
f_{yl}	=	yield stress of longitudinal reinforcement
f_{yw}	=	yield stress of transverse reinforcement
G	=	elastic shear modulus
GA_{eff}	=	initial shear stiffness
GA_A	=	current shear rigidity of the section at end A
GA_B	=	current shear rigidity of the section at end B
GA_o	=	shear rigidity at the intermediate part of the element
k	=	parameter depending on the curvature ductility demand
L	=	length of the member
L_s/h	=	shear span ratio
N	=	compressive axial load
s	=	spacing of transverse reinforcement
$V_{A,cr}$	=	shear cracking force at end A
$V_{B,cr}$	=	shear cracking force at end B

V_{cr}	=	shear cracking force
V_c	=	shear force resisted by the concrete resisting mechanisms
V_{uo}	=	undegraded shear strength
V_u	=	degraded shear strength
V_s	=	shear force resisted by stirrups
V_w	=	shear strength contributed by transverse reinforcement
V_y	=	shear force at flexural yielding
α	=	angle between the column axis and the line joining the centers of the flexural compression zones at the top and bottom of the column
α_A	=	flexural yield penetration coefficient at the end A
α_{As}	=	shear cracking penetration coefficient at the end A
α_B	=	flexural yield penetration coefficient at the end B
α_{Bs}	=	shear cracking penetration coefficient at the end B
γ_{cr}	=	average shear distortion at shear cracking
γ_s	=	average shear distortion after shear cracking
γ_u	=	average shear distortion at onset of stirrup yielding
γ_y	=	average shear distortion at flexural yielding
Δ_{max}^{fl}	=	flexural displacement at onset of stirrup yielding
Δ_{max}^{sh}	=	shear displacement at onset of stirrup yielding
Δ_{max}^{sl}	=	anchorage slip displacement at onset of stirrup yielding
Δ_{max}^{tot}	=	total displacement at onset of stirrup yielding
Δ_{shear}	=	shear displacement
ΔV	=	current shear force increment
Δ_y^{fl}	=	flexural displacement at first yielding of longitudinal reinforcement
Δ_y^{sl}	=	anchorage slip displacement at first yielding of longitudinal reinforcement
$\Delta\gamma$	=	current shear strain increment
θ	=	angle defined by the column axis and the direction of the diagonal compression struts
κ	=	modification factor taking into account the influence of axial load in calculating γ_u

λ	=	modification factor taking into account the influence of shear span ratio in calculating γ_u
μ_φ	=	curvature ductility demand
ν	=	normalized compressive axial load
φ_y	=	curvature of the critical cross section at first yielding of longitudinal reinforcement

REFERENCES

1. Takayanagi, T., Derecho, A.T., Gorley, W.G. Analysis of Inelastic Shear Deformation Effects in Reinforced Concrete Structural Wall Systems. *Proc. Nonlinear Design of Concrete Structures, CSCE-ASCE-ACI-CEB International Symposium,* Univ. of Waterloo, Ontario, Canada, 1979.
2. Thom, C.V. The Effects of Inelastic Shear on the Seismic Response of Structures. *PhD Thesis*, University of Auckland, New Zealand, 1983.
3. Filippou, F.C., Ambrisi, A., Issa, A. Nonlinear Static and Dynamic Analysis of R/C Subassemblages. *Report UCB/EERC-92/08*, Univ. of California, Berkeley, 1992.
4. D'Ambrisi, A., Filippou, F.C. Correlation Studies on an RC Frame Shaking-table Specimen. *Earthquake Engineering & Structural Dynamics* 1997; **26**: 1021-1040.
5. Ricles, J.M., Yang, Y.S., Priestley, M.J.N. Modeling Nonductile R/C Columns for Seismic Analysis of Bridges. *J. of Struct. Eng.* 1998; **124**(4): 415-425.
6. Petrangeli, M., Pinto, P., Ciampi, V. Fiber Element for Cyclic Bending and Shear of R/C Structures. I: Theory. *J. of Eng. Mechanics* 1999; **125**(9): 994-1001.
7. Pincheira, J., Dotiwala, F., Souza, J. Seismic Analysis of Older Reinforced Concrete Columns. *Earthquake Spectra* 1999; **15**(2): 245-272.
8. Lee, D.H., Elnashai, A.S. Seismic Analysis of R/C Bridge Columns with Flexure-Shear Interaction. *J. of Struct. Eng.* 2001; **127**(5): 546-553.
9. Elwood, K., and Moehle, J.P. Shake Table Tests and Analytical Studies on the Gravity Load Collapse of RC Frames. *PEER Report No. 2003/01,* Univ. of California, Berkeley, 2003.
10. Cosenza, E., Manfredi, G., Verderame G. A Fibre Model for Pushover Analysis of Underdesigned R/C Frames. *Computers and Structures* 2006; **84**: 904-916.

11. Vecchio, F.J., Collins, M.P. The Modified Compression Field Theory for Reinforced Concrete Elements Subjected to Shear. *ACI Struct. J.* 1986; **83**(2): 219-231.
12. Hsu, T.T.C. Softened Truss Model Theory for Shear and Torsion. *ACI Struct. J.* 1988; **85**(6): 624-635.
13. Priestley, M.J.N., Seible, F., Calvi, G.M. *Seismic Design and Retrofit of Bridges.* Wiley: New York, 1996.
14. Priestley, M.J.N., Verma, R., Xiao, Y. Seismic shear strength of reinforced concrete columns. *Journal of Structural Engineering* 1994; **120**(8): 2310-2329.
15. Oesterle, R.G., Fiorato, A.E., Aristizabal - Ochoa, J.D., Corley, W.G. Hysteretic Response of Reinforced Concrete Structural Walls. *Proc. ACISP-63: Reinforced Concrete Structures subjected to Wind and Earthquake Forces*, Detroit, 1980.
16. Saatcioglu, M., Ozcebe, G. Response of Reinforced Concrete Columns to Simulated Seismic Loading. *ACI Struct. J.* 1989; **86**(1): 3-12.
17. Sivaselvan, M.V., Reinhorn, A.M. Hysteretic Models for Cyclic Behavior of Deteriorating Inelastic Structures. *Technical Report MCEER-99-0018*, University at Buffalo, State University of New York, 1999.
18. Park, Y.J., Reinhorn, A.M., Kunnath, S.K. Inelastic Damage Analysis of Reinforced Concrete Frame-Shear Wall Structures. *Tech. Report NCEER 87-0008*, State Univ. of New York at Buffalo, 1987.
19. Soleimani, D., Popov, E.P., Bertero, V.V. Nonlinear Beam Model for R/C Frame Analysis. *Proc. Seventh Conference on Electronic Computation*, ASCE, St Louis, Missouri, 1979.
20. Roufaiel, M.S.L., and Meyer, C. Analytical Modeling of Hysteretic Behavior of R/C Frames. *J. of Str. Eng.* 1987; **113**(3): 429-444.
21. Valles, R.E., Reinhorn, A.M., Kunnath, S.K., Li, C., Madan, A. IDARC2D Version 4.0: A Program for the Inelastic Damage Analysis of Buildings. *Technical Report NCEER-96-0010*, University at Buffalo, State University of New York, 1996.
22. Sezen, H., Moehle, J.P. Shear Strength Model for Lightly Reinforced Concrete Columns. *J. of Struct. Eng.* 2004; **130**(11): 1692-1703.

23. Ozcebe, G., Saatcioglu, M. Hysteretic Shear Model for Reinforced Concrete Members. *J. of Struct. Eng.* 1989; **115**(1): 132-148.

24. Park, R., Paulay, T. *Reinforced Concrete Structures.* Wiley: New York, 1975.

25. Kowalsky, M.J., Priestley, M.J.N. Shear Behavior of Lightweight Concrete Columns under Seismic Conditions. *Report No. SSRP-95/10,* University of San Diego, California, 1995.

26. Priestley, M.J.N., Seible, F., Verma, R., Xiao, Y. Seismic Shear Strength of Reinforced Concrete Columns. *Report No. SSRP-93/06,* Univ. California, San Diego, 1993.

27. Sezen, H. Seismic Behavior and Modeling of R/C Building Columns, *PhD Thesis*, University of California, Berkeley, 2002.

28. *fib* TG 7.1. *Seismic Assessment and Retrofit of R/C Buildings* (fib Bulletin 24); *Lausanne, 2003.*

29. CEN (European Committee for Standardization). *Eurocode 8: Design of Structures for Earthquake Resistance - Part 3: Assessment and retrofitting of buildings* (EN 1998-3:2005); Brussels, 2005.

30. Arakawa, T., Arai, Y., Egashira, K., Fujita, Y. Effects of the Rate of Cyclic Loading on the Load-Carrying Capacity and Inelastic Behavior of Reinforced Concrete Columns. *Transactions of the Japan Concrete Institute* 1982; **4**: 485-492.

31. Umehara, H., Jirsa, J.O. Shear Strength and Deterioration of Short Reinforced Concrete Columns Under Cyclic Deformations. *PMFSEL Report No. 82-3,* Department of Civil Engineering, University of Texas at Austin, 1982.

32. Bett, B., Klingner, R., Jirsa, J. O. Behavior of Strengthened and Repaired Reinforced Concrete Columns under Cyclic Deformations. *PMFSEL Report No. 85-3,* Department of Civil Engineering, University of Texas at Austin, 1985.

33. Aboutaha, R., Engelhardt, D., Jirsa, J., Kreger, E. Rehabilitation of Shear Critical Concrete Columns by Use of Rectangular Steel Jackets. *ACI Struct. J.* 1999; **96** (1): 68-77.

34. Xenos, A., Kappos, A.J. A Distributed Shear Flexibility Model for Seismic Damage Assessment of Reinforced Concrete Structures. *Proc. 11th European Conference on Earthquake Engineering*, Balkema, Rotterdam, 1998.

35. Lehman, D., Moehle, J.P. Seismic Performance of Well Confined Concrete Bridge Columns. *PEER Report 1998/01*, Univ. of California, Berkeley, 1998.

36. Lynn, A., Moehle, J.P., Mahin, S., Holmes, W. Seismic Evaluation of Existing Reinforced Concrete Building Columns. *Earthquake Spectra* 1996; **12**(4): 715-739.

37. Biskinis, D., Roupakias, G., Fardis, M.N. Degradation of Shear Strength of R/C Members with Inelastic Cyclic Displacements. *ACI Struct. J.* 2004; **101**(6): 773-783.

Table 1. Values of γ_u determined on the basis of available experimental V-Δ_{shear} envelope curves

Specimen	**Reference**	**ν**	**L_s/h**	**γ_u (‰)**
C5A	Priestley et al. [26]	0.06	2	5.4
SL1	Kowalsky et al. [25]	0.04	2	4.4
2CLD12	Sezen [27]	0.15	3.2	2.7
2CHD12	Sezen [27]	0.60	3.2	1.0
2CLD12M	Sezen [27]	0.15	3.2	3.3

Table 2. Values of γ_u determined using the proposed procedure

Specimen	**Reference**	**ν**	**L_s/h**	**γ_u (‰)**
OA2	Arakawa et al. [30]	0.18	1.25	4.56
CUS	Umehara et al. [31]	0.16	1.11	9.03
2CUS	Umehara et al [31]	0.27	1.11	7.11
No 1-1	Bett et al. [32]	0.10	1.50	5.10
SC9	Aboutaha et al. [33]	0.00	1.33	5.54

FIGURE CAPTIONS

Figure 1: Flexural sub-element

Figure 2: Primary curve without degradation for shear force vs. shear deformation

Figure 3: Comparison of analytical predictions with experimental values of γ_u (‰)

Figure 4: Relationship between curvature ductility demand and strength of concrete shear resisting mechanisms (Priestley et al. 1994)

Figure 5: Shear-flexure interaction procedure

Figure 6: Derivation of shear primary curve after modeling shear-flexure interaction effect: (a) Flexural primary curve in terms of member shear force and curvature ductility demand of the critical cross section; (b) shear ($V - \gamma$) primary curve after modeling shear-flexure interaction

Figure 7: Developments regarding unloading branches: (a) Average unloading stiffness; (b) minimum unloading stiffness

Figure 8: Cases of numerical instability during reloading: (a) Reference point (P) below cracking load; (b) reference point (P) slightly above cracking load

Figure 9: Shear sub-element: (a) Dominant gravity loading; (b) Dominant seismic loading

Figure 10: Lehman et al. (1998) specimen 415: (a) Lateral load vs. total displacement; (b) Shear demand and shear capacity vs. curvature demand of the end section; (c) Shear force vs. shear strain hysteresis loops; (d) Time history of displacement components

Figure 11: Lynn et al. (1996)] specimen 2CLH18: (a) Lateral load vs. total displacement; (b) Shear demand and shear capacity vs. curvature demand of the end section; (c) Shear force vs. shear strain hysteresis loops; (d) Time history of displacement components

Figure 12: Aboutaha et al. (1999) specimen SC9: (a) Lateral load vs. total displacement; (b) Shear force vs. shear strain hysteresis loops; (c) Lateral load vs. total displacement relationship, without modeling shear; (d) Time-history of displacement components

FIGURES

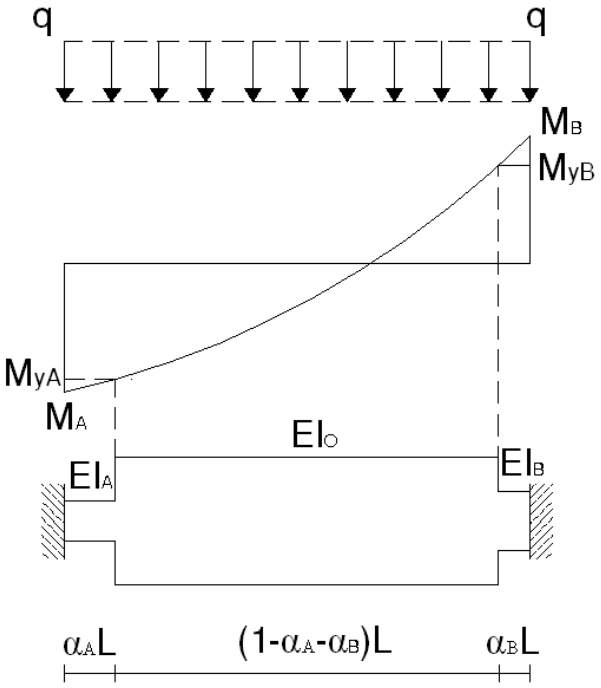

Figure 1: Flexural sub-element

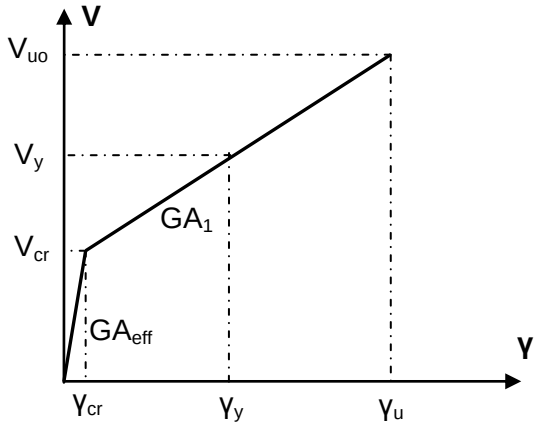

Figure 2: Primary curve without degradation for shear force vs. shear deformation

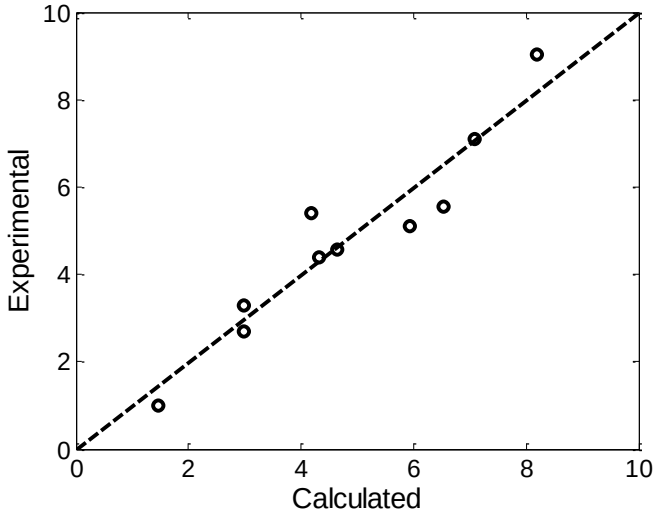

Figure 3: Comparison of analytical predictions with experimental values of γ_u (‰)

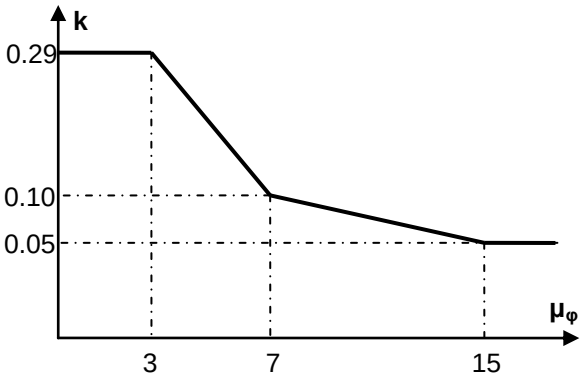

Figure 4: Relationship between curvature ductility demand and strength of concrete shear resisting mechanisms (Priestley et al. [14])

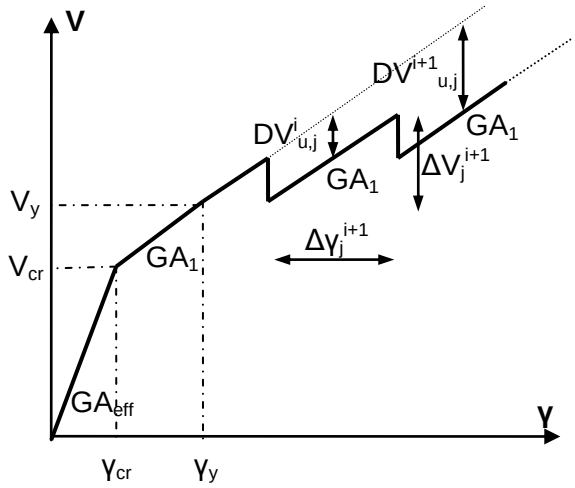

Figure 5: Shear-flexure interaction procedure

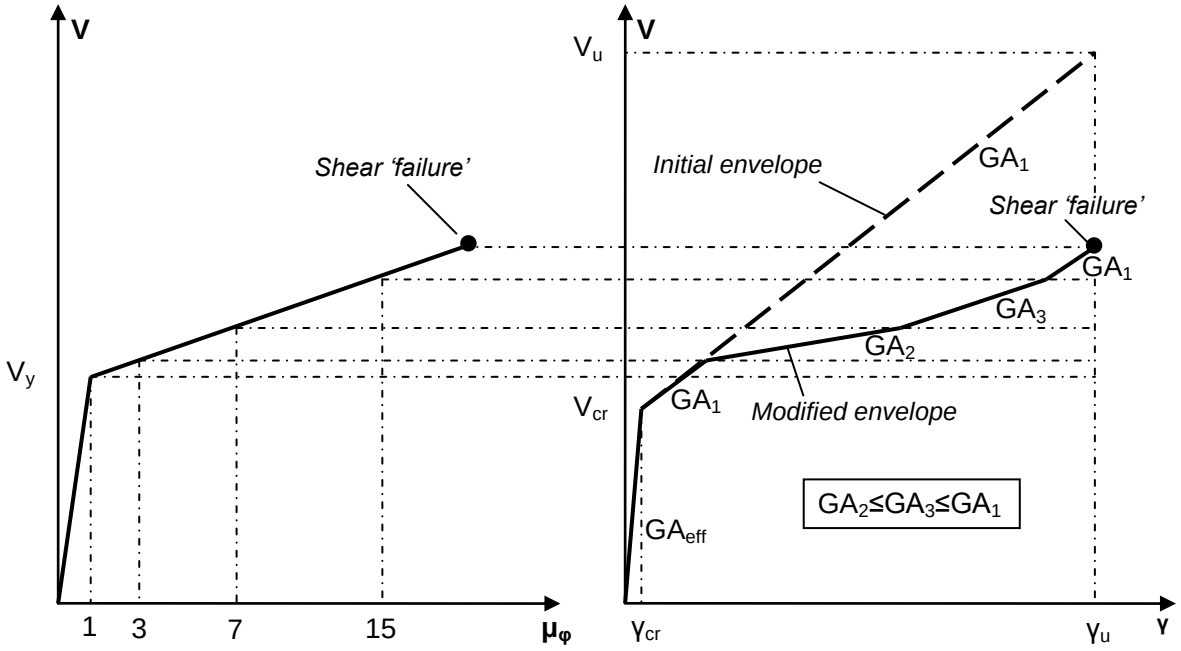

Figure 6: Derivation of shear primary curve after modeling shear-flexure interaction effect: (a) Flexural primary curve in terms of member shear force and curvature ductility demand of the critical cross section; (b) shear (V – γ) primary curve after modeling shear-flexure interaction

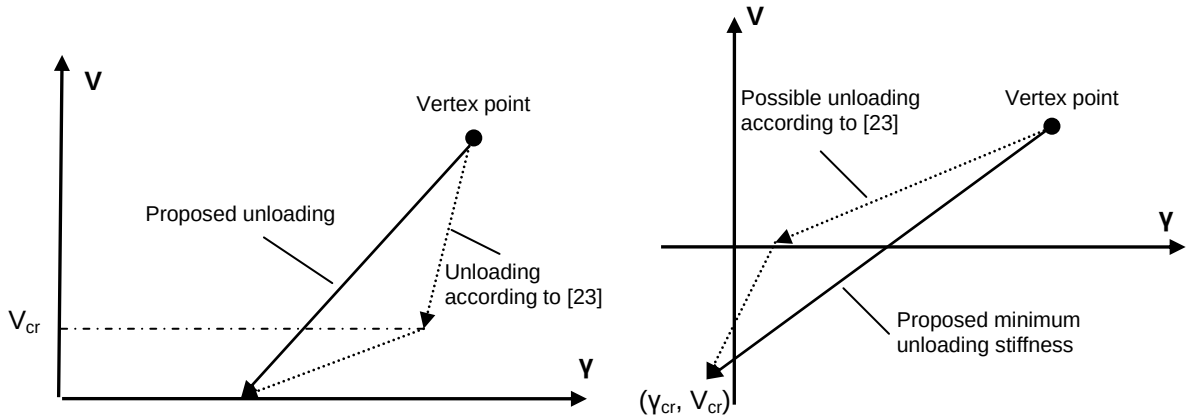

Figure 7: Developments regarding unloading branches: (a) Average unloading stiffness; (b) minimum unloading stiffness

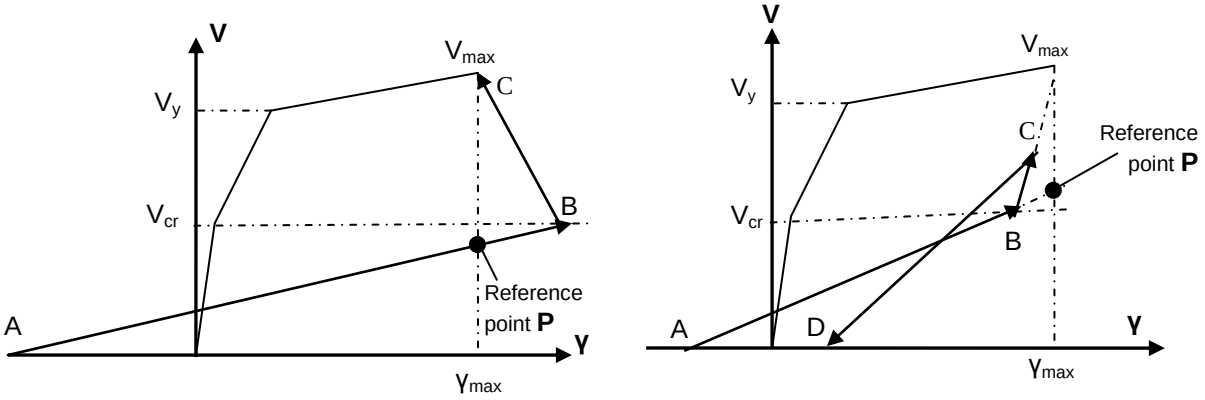

Figure 8: Cases of numerical instability during reloading: (a) Reference point (P) below cracking load; (b) reference point (P) slightly above cracking load

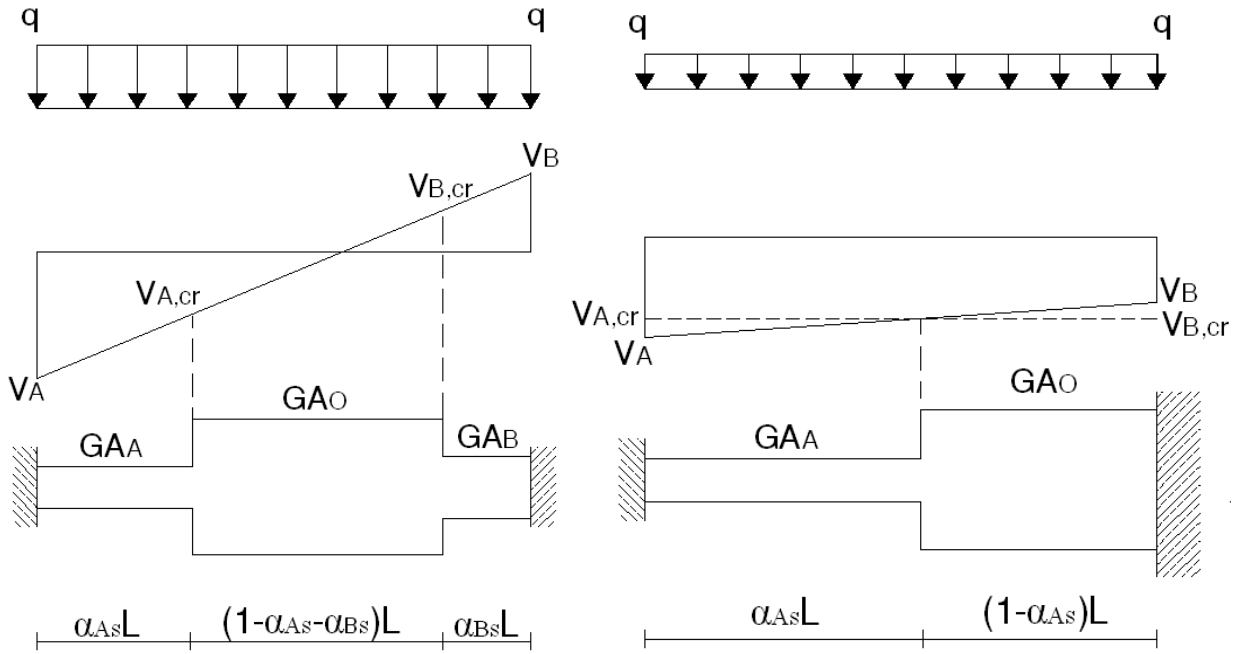

Figure 9: Shear sub-element: (a) Dominant gravity loading; (b) Dominant seismic loading

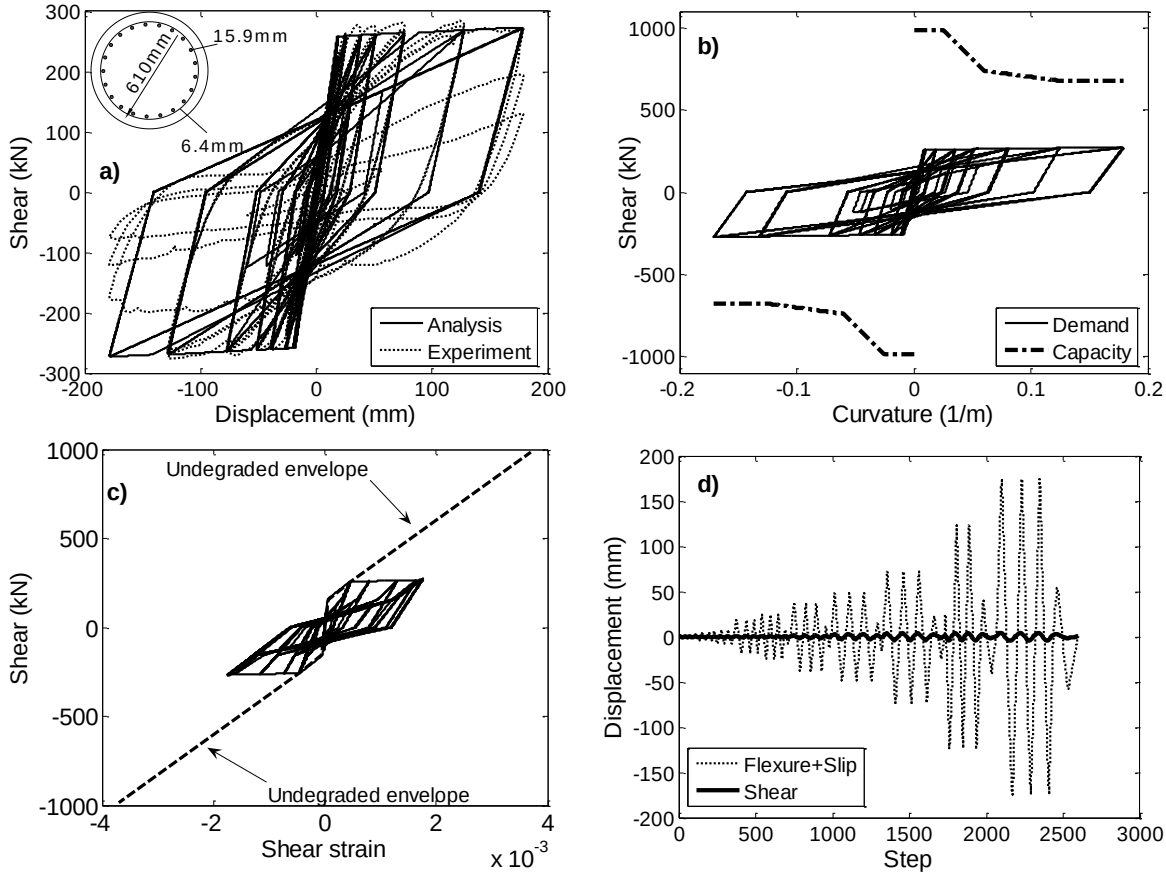

Figure 10: Lehman et al. (1998) specimen 415: (a) Lateral load vs. total displacement; (b) Shear demand and shear capacity vs. curvature demand of the end section; (c) Shear force vs. shear strain hysteresis loops; (d) Time history of displacement components

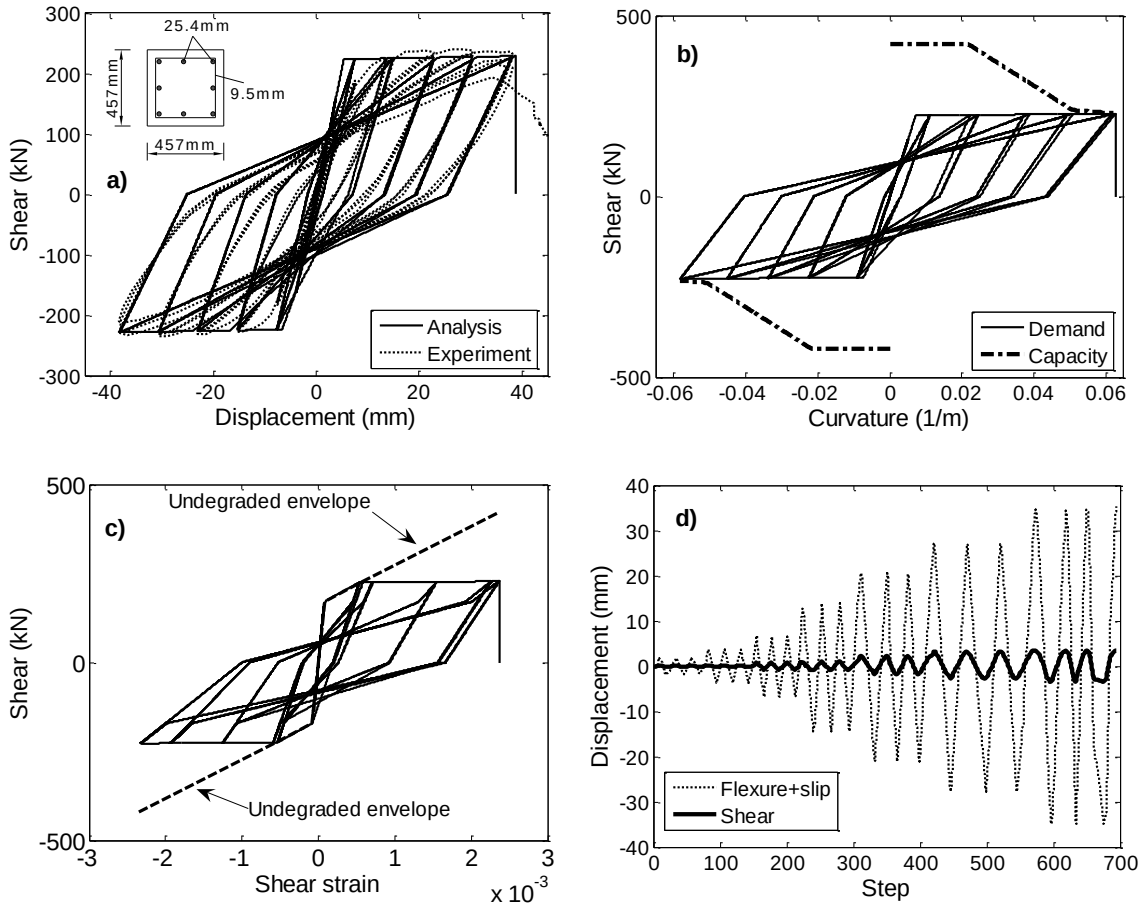

Figure 11: Lynn et al. (1996)] specimen 2CLH18: (a) Lateral load vs. total displacement; (b) Shear demand and shear capacity vs. curvature demand of the end section; (c) Shear force vs. shear strain hysteresis loops; (d) Time history of displacement components

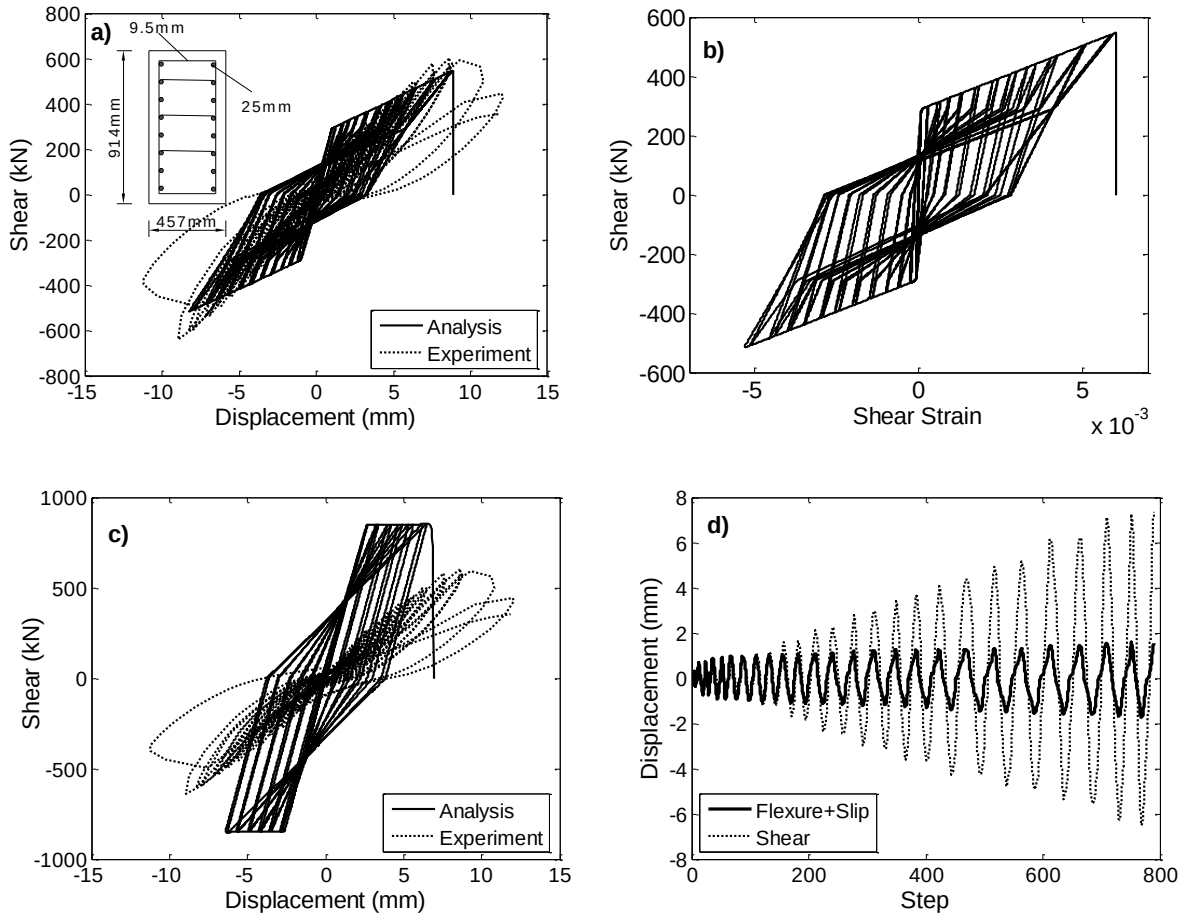

Figure 12: Aboutaha et al. (1999) specimen SC9: (a) Lateral load vs. total displacement; (b) Shear force vs. shear strain hysteresis loops; (c) Lateral load vs. total displacement relationship, without modeling shear; (d) Time-history of displacement components